Tutora

Dra. Elena Cerdeiras Montero
Departament de Química Inorgànica

Grau de Química

Treball Final de Grau

Synthesis and study of new piezoelectric $(Bi_{0.5}Na_{0.5})TiO_3$-$BaTiO_3$ based materials

Marc Nogueras Garcia

June 2017

UNIVERSITAT DE BARCELONA

B:KC Barcelona Knowledge Campus
Campus d'Excel·lència Internacional

I would like to thanks my degree's final project director Elena Cerdeiras for all her patience and for being there every time I needed her, also for her severe corrections that has given me big headaches but has helped the work to look quite professional. I couldn't also had made this work without the help of Lourdes Mestres, who has showed me throughout what means to investigate and the thrilling of discovering and has guided me when I didn't know where to go.

For this and more, I don't think I could have hoped for better laboratory company. Thanks for all the work you have done on me and I just want you to know I have really enjoyed my time here on the Solid State Chemistry group as a researcher.

REPORT

CONTENTS

1. SUMMARY 3
2. RESUM 5
3. INTRODUCTION 7
3.1. Theory basics 8
3.1.1. Piezoelectricity and ferroelectricity 8
3.1.2. Solid state chemistry 10
3.1.3. Solid state reaction 11
3.1.4. Perovskite structure 11
3.1.5. $Bi_{0.5}Na_{0.5}TiO_3$-$BaTiO_3$ 13
3.1.6. Effects of doping BNT-BT 14
3.2. Characterization techniques 15
3.2.1. Thermal Analysis (TGA – DTA) 15
3.2.2. Infrared Spectroscopy (IR) 15
3.2.3. X-Ray Diffraction (XRD) 16
3.2.4. Scanning Electron Microscopy (SEM) 19
3.2.5. Energy Dispersive X-Ray Spectroscopy (EDS) 19
3.2.6. Impedance Spectroscopy (IS) 20
4. OBJECTIVES 21
5. EXPERIMENTAL SECTION 22
6. RESULTS AND DISCUSSION 29
6.1. X-Ray Diffraction (XRD) 29
6.2. Scanning Electron Microscopy–Energy Dispersive X-Ray Spectroscopy (SEM/EDS) 34
6.3. Impedance Analysis (IS) 39
7. CONCLUSIONS 50
8. REFERENCES AND NOTES 51

1. SUMMARY

Piezoelectric materials based on lead zirconate titanate (PZT) are widely used in a large number of electronic devices due to their excellent properties. This improvement occurs in a region of the phase diagram related to a morphotropic phase boundary (MPB). However, the major drawback is the environmental and health problems arising from the presence of lead due to its high toxicity. Therefore, nowadays and during last years, the scientific community has focused on the search for lead-free piezoelectric materials.

($Bi_{0.5}Na_{0.5}$)TiO_3-$BaTiO_3$ based ceramics (BNT-BT) has attracted considerable interest attributable to their similar characteristics to PZT. This system has a morphotropic phase boundary where a great piezoelectric response is obtained and, for this reason, BNT-BT system is considered a promising candidate to replace lead-based piezoelectric materials. However, even with the large number of studies carried out there is no exact composition around MPB where the best properties are obtained. So, it is necessary to continue doing research and try to improve the functional properties.

Hence, the goal of this work has been the study of different aspects associated with ($Bi_{0.5}Na_{0.5}$)TiO_3-$BaTiO_3$ system based ceramic materials.

In this work, the preparation of BNT-BT based ceramics has been made by solid state reaction and their characterization has been carried out with the different techniques used on solid state chemistry. The planetary ball mill has been stablished as an important part of the synthesis pathway and optimizing the sintering conditions has been done. High density ceramics have been obtained in all compositions with a relative density around 98%. In all cases, perovskite unique phase ceramics have been obtained with coexistence of rhombohedric and tetragonal phase, confirming that they are on the morphotropic phase boundary. Using Scanning Electron Microscopy, the presence of a BNT matrix with grains of BT on the obtained ceramics has been observed.

In order to improve the functional properties of these materials, the effect of lanthanide donor dopants has been studied, focusing on the influence of different radius and their concentration. Through X-Ray Diffraction the introduction of dopants on the BNT-BT structure has been confirmed since the diffraction maximums have been shifted to higher angles, meaning the incorporation of lower radius cations and the creation of cationic vacancies. The introduction of Lanthanum has provoked a morphologic variation of the barium titanate grains, which leads us to

believe that Lanthanum has been introduced on the $BaTiO_3$ structure, as it was expected due to the stoichiometry of the compound.

The dielectric properties of BNT-BT based ceramics have been studied on the morphotropic phase transition, obtaining high values of relative permittivity for the non-doped ceramic and low dielectric losses in all compositions. The Praseodymium doped BNT-BT shows a dielectric behavior dependent on frequency at room temperature, both related to relative permittivity and dielectric losses, better than the non-doped BNT-BT.

Keywords: piezoelectric material, lead-free, processing, ceramics, donor doping, functional properties.

2. RESUM

Els materials piezoelèctrics basats en el titanat zirconat de plom (PZT) són àmpliament utilitzats en una gran quantitat de dispositius electrònics degut a les seves excel·lents propietats elèctriques. Aquesta millora de les propietats té lloc en certa regió del diagrama de fases que es denomina transició de fase morfotrópica i depèn de la composició. No obstant, el gran inconvenient que presenta és la presència de plom degut a la seva elevada toxicitat, perjudicial per la salut i el medi ambient. Per tant, en l'actualitat i durant el últims anys, la comunitat científica ha centrat el seu interès en la recerca de nous materials piezoelèctric lliures de plom capaços de substituir el PZT.

Les ceràmiques basades en $(Bi_{0.5}Na_{0.5})TiO_3$-$BaTiO_3$ (BNT-BT) ha despertat un considerable interès ja que presenta característiques similars a les del PZT i és respectuós amb el medi ambient. Aquest sistema presenta una transició de fase morfotròpica on s'obté una bona resposta piezoelèctrica i, per tant, és considerat un candidat prometedor per substituir els materials piezoelèctrics basant en plom. Encara així, és important destacar que s'han dut a terme un gran nombre d'estudis d'aquest sistema però no existeix una composició exacta al voltant de la regió de la transició de fase morfotròpica en la que s'obtenen les millors propietats. Per tant, es necessari continuar investigant sobre aquest material i intentar millorar les propietats funcionals.

Així, l'objectiu d'aquest treball ha estat l'estudi de diferents aspectes relacionats amb materials ceràmics basant en el sistema $(Bi_{0.5}Na_{0.5})TiO_3$-$BaTiO_3$.

En aquest treball, s'ha dut a terme la preparació per reacció en estat sòlid de ceràmiques basades en BNT-BT i la seva caracterització mitjançant les diferents tècniques utilitzades en la química de l'estat sòlid. S'ha establert la utilització del molí de boles com una part important de la ruta de síntesis i s'ha dut a terme la optimització de les condicions de sinterització. S'han obtingut ceràmiques d'alta densitat en totes les composicions amb una densitat relativa al voltant del 98%. En tots els casos, s'han obtingut ceràmiques amb fase única de tipus perovskita amb coexistència de fase romboèdrica i tetragonal, confirmant que es troben a la regió de la transició de fase morfotròpica. Mitjançant microscòpia electrònica de rastreig, s'ha observat la presència d'una matriu de grans de BNT amb grans de BT a les ceràmiques obtingudes.

Amb la finalitat de millorar les propietats funcionals d'aquests materials, s'han estudiat els efectes dels lantànids com a dopants donadors, centrant-se en la influència dels diferents radis i

la seva concentració. Mitjançant difracció de raigs X s'ha aconseguit confirmar la introducció dels diferents dopants dins l'estructura del BNT-BT degut al desplaçament dels màxims de difracció cap a angles més grans, consistent amb la incorporació de cations de radi menor i amb la creació de vacants catiòniques. La introducció del lantani ha provocat una variació morfològica dels grans del titanat de bari, el que ens porta a pensar que s'ha introduït a l'estructura del $BaTiO_3$, tal i com s'esperava per l'estequiometria del compost.

S'han estudiat les propietats dielèctriques de les ceràmiques basades en el BNT-BT a la transició de fase morfotròpica, obtenint-se uns valors alts de permitivitat relativa per la ceràmica sense dopar i unes pèrdues dielèctriques baixes en totes les composicions. El BNT-BT dopat amb praseodimi mostra un comportament dielèctric dependent de la freqüència a temperatura ambient, tant relatiu a la permitivitat com a les pèrdues dielèctriques, més bo que la ceràmica de BNT-BT sense dopar.

Paraules clau: material piezoelèctric, lliure de plom, preparació, ceràmiques, dopatge donador, propietats funcionals.

3. INTRODUCTION

Piezoelectric materials have a wide range of applications. Since the material oscillates at a certain frequency when an alternating voltage is applied, it can make a membrane vibrate generating sound and is used for all the types of speakers, subwoofers and headphones. If a mechanical stress is applied generates voltage and is used in microphones, lighter flint stones and more. Other uses include all types of radars, all sensors, computer hard drives and USB memories, touch screen displays and even injectors of motors.

The piezoelectric effect was discovered back on 1600 by Elie Seignette who prepared a sodium potassium tartrate, La Rochelle salt, named after the place where it was discovered, La Rochelle in France (1). Then 200 years passed without any new studies until, on 1824, David Brewster observed the pyroelectric effect on La Rochelle salts (2). But the first documented works about piezoelectricity were made by Jacques and Pierre Curie back on 1880, they established the direct piezoelectric effect and the inverse piezoelectric effect (3).

Many materials can exhibit piezoelectricity, many of them are natural crystals like quartz, tourmaline and sodium potassium tartrate. All these materials are dielectric and have been used extensively during years as electromechanical transducers. The study presented in this work will be centered on the piezoelectric polycrystalline ceramics, which are ceramics that, once poled, present piezoelectric properties. Piezoelectric ceramics are hard, chemically inert and completely insensitive to humidity or other atmospheric influences. Their mechanical properties resemble those of the known ceramic insulators (4).

The most used piezoelectric ceramic is PZT, lead zirconate titanate, because of its excellent properties as a piezoelectric. This material was discovered on 1954 by B. Jaffe (5) and has been the most important piezoelectric in the industry. As this material contains more than half of his weight of lead, which is a highly toxic and volatile element, and at sintering process lead oxide is released to the atmosphere, research has been focused on obtaining lead-free piezoelectric materials that are environmentally friendly. One of the main option is bismuth sodium titanate – barium titanate, $(Bi_{0.5}Na_{0.5})TiO_3$-$BaTiO_3$ (BNT-BT). Sodium is not harmful nor it is the barium and bismuth is a heavy metal but, unlike most of them, it is not harmful for the living beings or toxic. BNT-BT based materials are polycrystalline piezoelectric with perovskite crystal structure and show interesting properties.

In this essay, BNT-BT based ceramics were prepared to study the effect of modifications on synthesis route on the functional properties and was doped with different Lanthanides to study their dielectric properties. All the compounds were prepared following the solid state method.

3.1. THEORY BASICS

The objective of this part is to introduce the concepts of the synthesis and the characterization of the piezoelectric material.

3.1.1. Piezoelectricity and ferroelectricity

Piezoelectric materials are those that exhibit the piezoelectric effect, either naturally or when poled. The direct piezoelectric effect is described as the ability of certain materials to generate an electric charge in response to an applied mechanical stress. The same materials can also be deformed when they are exposed to an electric field, which is known as the inverse piezoelectric effect. These materials do not have center of symmetry so a stress (tensile or compressive) applied to such a crystal will alter the separation between the positive and negative charged sites in each elementary cell leading to a net polarization at the crystal surface. The effect is practically linear, the polarization varies directly with the applied stress, and is direction-dependent (anisotropic), so that compressive and tensile stress will generate electric fields and hence voltages of opposite polarity. This effect is reciprocal, so that if the crystal is exposed to and electric field, an elastic strain will be observed, causing to vary the length according to the field polarity. The direct piezoelectric effect is known as generator or sensor effect and the inverse piezoelectric effect is known as the actuator effect (4).

All piezoelectric materials are dielectric, which means they are insulators. Inside the piezoelectric materials there are subgroups, in this case the pyroelectric materials which are the materials that can transform the calorific energy to electric energy, hence if heated electricity is generated because their crystallographic axis with spontaneous polarization can change with the temperature. Inside the pyroelectric materials there us a subgroup which are the ferroelectric materials. Ferroelectric materials are those that can inverse their spontaneous polarization if an electric field is applied. All this phenomena are related to the crystalline structure of the materials, so the symmetry of the crystals effects on their physics external properties and it is ruled by the Neumann Principle (6).

Above the temperature known as the Curie point, the crystallites exhibit simple cubic symmetry, hence becoming centrosymmetric and losing the ability to generate dipoles because the positive and negative charged sites coincide. Below that temperature, the dipole in each elementary cell can be reversed and switched by the application of an electric field. These materials are ferroelectric, they are anisotropic, which means that the electric and mechanic properties of the material have different direction from the applied force.

The dipoles inside the material are not randomly oriented, neighbouring dipoles align themselves in the same direction forming local alignment regions knows as domains. Outside this domains, the net dipole moment of the material is random because the domains are randomly oriented so there is no polarization. If the material is exposed to a strong electric field under the Curie point temperature, the domains will tend to align to the electric field giving the material a net polarization. When an electric field is applied, the domains preferably oriented to the field grow and the ones that have unfavorable orientation shrink and the material will lengthen in the direction of the field. As it can be seen, domains may vary on dimensions but the crystalline defects anchor these domains. There is a moment when all the domains are oriented to the field direction and this is called the saturation polarization, *Ps*, as seen in figure 1. If a mechanical stress is applied on the material, being tensile or compressive, electric field will be generated. The volume of the material does not change so if we apply an inverse voltage of the one applied for poling, the material will deform causing the length to change depending on the voltage applied (7).

Once polarized, and removed the external electric field, the dipoles become less aligned but do not return to the original alignment because they are bound to a certain preferred direction within the individual crystallites and remain to the preferred direction most close to the alignment of the applied electric field. So the net polarization is lower than the polarization at the saturation point but is still high and it is known as the remanent polarization, *Pr*. If an opposite direction voltage is applied, the domains will align to this voltage until all of them are aligned arriving to the saturation polarization point. If this is plotted is called the hysteresis curve, plotting E vs P, as seen in figure 1. The coercive field, Ec, is the electric field needed to apply to get the remanent polarization to zero, the lower the better for many applications since it will be easier to polarize and unpolarize.

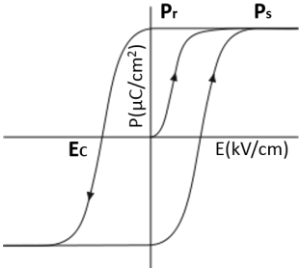

Figure 1: Hysteresis curve of ferroelectric materials.

Ferroelectric materials present anomalies with temperature in their dielectric constant, ε', presenting a maximum value on the phase transition, corresponding to a transition to paraelectric phase. This variation of the permittivity in function of the temperature can have three different transitions. The maximum observed on figure 2a corresponds to a normal phase transition but, for some materials, if the peak is wide corresponds to a diffuse phase transition, figure 2b, and the last group are the materials that have a wide peak and also are frequency dependent, these materials are labeled as relaxor, as BNT-BT or PZT, as seen in figure 2c.

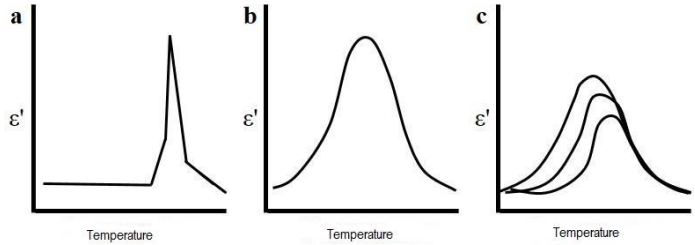

Figure 2: Different types of phase transitions. a. Normal phase transition, b. Diffuse phase transition, c. Relaxor phase transition

3.1.2. Solid state chemistry

Solid state chemistry is concerned with the synthesis, structure, properties and applications of solid materials. The solid state chemistry describes and classifies the crystalline structures, or the amorphous ones, of the solids and studies the factors that control and influence this structures like the structural defects that vary the conductivity, mechanical properties and chemical reactivity.

3.1.3. Solid state reaction

They are based on synthetizing solids from reagents with no solvents involved heating a mixture of solid precursors at high temperatures in order to make the reaction possible.

As obvious, the mobility of the ions in the solid is despicable so for the reactions to take place there is a need to facilitate as much as possible the encounter between the reactants and to apply the optimum reaction conditions to make the reactions possible, since they are thermodynamically possible but not kinetically. For facilitating the encounter of the reactants, normally oxides or carbonates, a reduction of the particle size must be made because surface contact and defects are enhanced and try to homogenize to facilitate the diffusion of the ions of the reactants.

The calcination of the reactants must be done on fine powder at high temperatures in order to enhance the diffusion during a large amount of time, some hours usually. The problem with the method is that the new phase grows at the grain boundaries and it blocks the diffusion between the reactants to form the new phase so homogenization of the reactants mixture by different milling processes must be done to solve the problem. Also the more similar the crystal structures of the reactants and products are, the easier it is to diffuse, is easier for an ion to jump from an octahedral hole to another octahedral hole than from an octahedral hole to a tetrahedral hole. It also applies to the cell structure, it is easier if the reactants have the same structure as the products because it will not take as much reorganization as if it has to change between crystal systems.

To obtain densified ceramics, sintering process is carried out to fill the holes that contain air that will affect the electric properties.

3.1.4 Perovskite structure

Most of piezoelectric materials have perovskite structure, like BNT-BT and PZT. The name was given after the name of a mineral, $CaTiO_3$, and all the family materials with general formula ABO_3 with the same structure share the name. This mineral was discovered by the German geologist Gustav Rose in 1839, who named it after the mineralogist Lev Aleksevigh von Perovski and was found on the Ural Mountains of Russia (8).

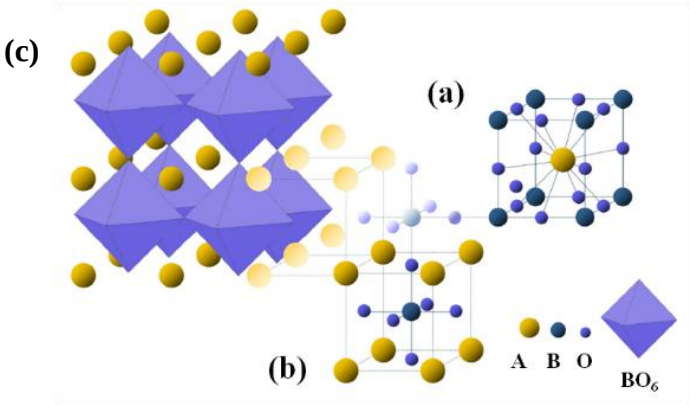

Figure 3: Different representations of the perovskite structure. a. Cation A centered cubic b. Cation B centered cubic. c. tridimensional representation of a BO_6 octahedron.

The perovskite structure could be described as a net of BO_6 octahedrons that share the six vertex with other octahedrons, figure 3c. A cations, the bigger ones, occupy interstitial positions with number of coordination 12 and B cations on the center of the octahedron occupy positions with coordination number 6, so B cations have smaller radius than A cations. It can also be described as seen on figure 3a, in which the A ion occupies the central position and the cubic vertices are occupied by B cations and the oxygen anions occupy the center of the edges. In figure 3b it is presented as a compact cubic structure for cation A and oxygen anions and B is on a quarter of the octahedral holes.

This would be the ideal perovskite structure, but in reality perovskite structure materials tend to have distortions and these distortions are what makes it have spontaneous polarization due to the atomic movement of A and B which results in lower symmetry structures (9)(10), figure 4.

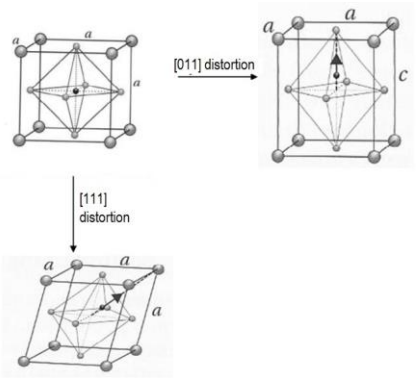

Figure 4: Distortion of the cubil cell to tetragonal and rhombohedral cells.

3.1.5. $Bi_{0.5}Na_{0.5}TiO_3$-$BaTiO_3$

Bismuth sodium titanate, $Bi_{0.5}Na_{0.5}TiO_3$-$BaTiO_3$, is a piezoelectric material with good properties which makes it one of the most solid candidates to substitute PZT in different applications. For being near as good as PZT we need to have certain similarities in the materials. The main similarity is the perovskite structure they share with BNT-BT. The other main similarity are the cations, both A cations that substitute Pb^{2+} have a couple of unpaired electrons, Bi^{3+}, and Na^{+}, maintains electroneutrality due to the charge excess on bismuth, and the unpaired electrons distort the unit cell and enhance the polarization.

PZT shows its superb properties near or on the MPB, the morphotropic phase boundary which is the region where it presents a structure change independent of temperature and that varies with composition and where tetragonal and rhombohedral structure coexist and (11). BNT has a rhombohedral structure *R3c* while BT shows a tetragonal *P4bm* structure at room temperature and this is why it is mixed together so it shows the MPB where it cohabitates rhombohedral and tetragonal structure. This MPB is around the 6-7% of $BaTiO_3$, figure 5 (11,12). BNT-BT shows two phase transitions, one at low temperature which corresponds to ferroelectric – antiferroelectric phase transition and another one at high temperature which is the antiferroelectric – paraelectric phase transition.

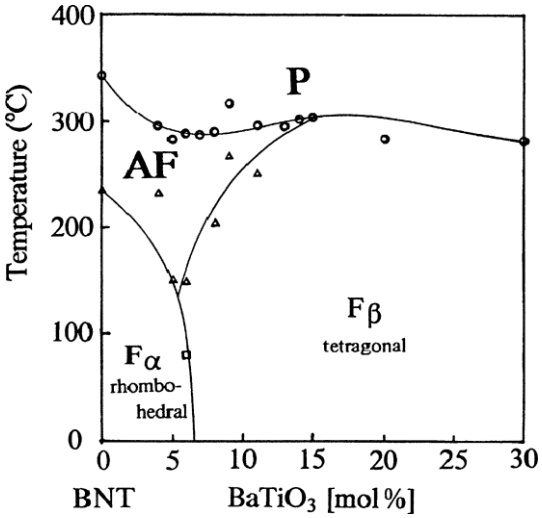

Figure 5:Phase diagram of (1-x) $(Bi_{0,5}Na_{0,5})TiO_3$-x$BaTiO_3$. P corresponds to paraelectric, AF to antiferroelectric, and F to ferroelectric. MPB is found between Fα and Fβ.

(Image extracted from T. Takenaka, K. Maruyama, K. Sakata; J. Appl. Phys. 30, 2236-2239 (1991))

BNT exhibits a high Curie temperature, which makes the material useful in a wide range of temperatures, and high remanent polarization but it also has a high coercive field, Ec, (13–15) which makes it more difficult to polarize but the 7% composition shows a relatively low Ec compared to other compositions, probably thanks to a major mobility of the domains. Also, the main problem with the structure is to maintain stoichiometry due to bismuth and sodium losses because of the volatilization of its oxides at the sintering process and sufficient losses makes the ceramic electrically conductive (16). BNT-BT shows aging effect, it doesn't have the ability to retain total remanent polarization after being polarized regularly, this effect appears to be dependent on barium titanate content since different values at room temperature are exhibited (17).

3.1.6. Effects of doping BNT-BT

A method that can be used to improve the properties of BNT-BT ceramics is to introduce a dopant element into the structure. If the doping ion has a higher oxidation state than the ion is substituting, the ion is a donor doping so it tends to give away the electrons of its outer shell, this is the one that may give interesting characteristics and it creates cationic vacancies. If the dopant

ion has a lower oxidation state than the substituted ion, is an acceptor dopant so it creates anionic vacancies.

In this essay, doping with Lanthanides is made because they are electron donors that create cationic vacancies, due to the cation substituted will be the one on A position of the perovskite, the barium cation, that is on 12 coordinated position by a La^{3+} or Pr^{3+} cation, which has a higher oxidation state than Ba^{2+}. The cation vacancies that the doping generates will modify the mobility of the domain walls so, in theory, the coercive field should be modified and it should change the remanent polarization and the permittivity and it also will modify the temperature of the phase transition. Also this doping should help the matter transportation during the sintering, making the ceramic more dense, and lower the size of the grains. As it was observed by Fu P., *et al* for the BNT-BT 0.06 (18).

3.2. CHARACTERIZATION TECHNIQUES

3.2.1. Thermal analysis (TGA – DTA)

Thermal analysis is the analysis of the physical and chemical properties of a sample as a function of temperature. These technique let us determine the phase diagrams and study the phase transitions. Inside these analysis, TGA and DTA techniques have been used.

TGA stands for termogravimetric analysis and measures the weight variation of the sample varying temperature or time, leaving a fixed temperature. The initial and ending temperature of a process is related to the grain size, heating conditions and the atmosphere where it takes place.

DTA stands for differential thermal analysis between a sample and a reference, which does not have phase transitions or weight losses in the studied range of temperatures, and the results are compared to see the endothermic ($\Delta T<0$) or exothermic ($\Delta T>0$) processes and to see if the processes are reversible or irreversible. The sample is heated and cooled down until the initial temperature and the thermal hysteresis graphic is obtained.

3.2.2. Infrared spectroscopy (IR)

When infrared radiation interacts with atoms it excites its vibrational states due to its characteristic wavelength, due to this the absorption of radiation in this range can be related to

the symmetry and structure of compounds. So infrared spectroscopy is a useful technique for structural determination.

The absorption of this radiation depends on the mass of the atoms and the strength of the bonding, so this technique let us determine the formation of a new phase and whether or not we have a single phase in our compound.

All the infrared spectra from the studied compounds were obtained with the equipment *Thermo Nicolet Avatar 330 FT-IR,* with a frequency range from 4000 to 400 cm^{-1}, from the *Departament de Química Inorgànica i Orgànica, secció Química Inorgànica*. The obtained data was treated with the computer program *OMNIC*. The pellets were a mixture of our compound and KBr.

3.2.3. X-Ray Diffraction (XRD)

XRD is the most used and most useful characterization technique in solid state chemistry. The technique is based on the diffraction that occurs when X-Rays collide over the successive planes of a crystal. This phenomena happens when electrons are accelerated through 30000 V and collide with matter, these electrons are slowed down or stopped by the collision and some of their lost energy is converted into X-Ray, in this case the electrons collide with a metal target of copper. These electrons can ionize some of the copper 1s (K shell) and an electron of an outer orbital (2p or 3p) drops down to occupy the vacant 1s level and the energy released in the transition appears as X-radiation, as seen in figure 7. For copper, the 2p → 1s transition, called Kα, as seen in figure 6, has a wavelength of 1.5418 Å which in fact is a doublet, $K\alpha_1$ = 1.54051 Å and $K\alpha_2$ = 1.54433 Å because the transition has different energy for the two possible spin states of the 2p electron. This makes the X-Rays that hit the sample monochromatic so only $K\alpha_1$ and $K\alpha_2$ hit it. There is another important transition, the 3p → 1s, which is Kβ but it is much more infrequent and less intense so it is not much used.

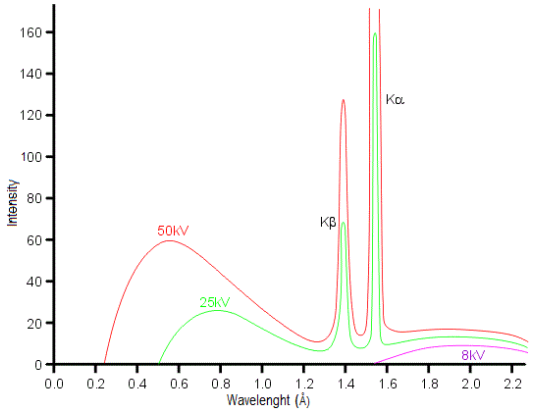

Figure 6: X-Ray spectrum for copper

(image extracted from School of Crystallography, Birkbeck College, University of London; http://pd.chem.ucl.ac.uk/pdnn/inst1/filters.htm; March 2017)

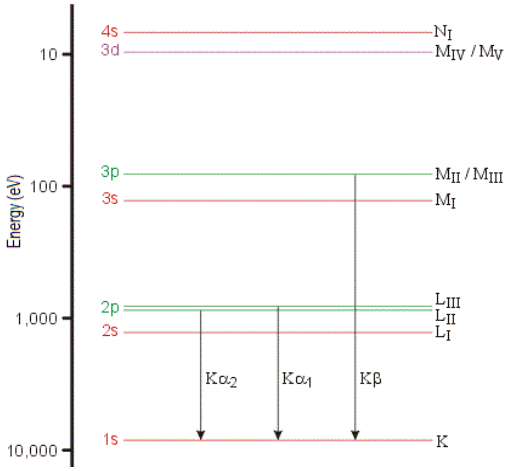

Figure 7: Electronic energy levels for a copper atom

(image extracted from School of Crystallography, Birkbeck College, University of London; http://pd.chem.ucl.ac.uk/pdnn/inst1/filters.htm; March 2017)

When the X-Ray beam passes through the sample it is diffracted by the different crystallographic planes in many directions and only the beams that have constructive interferences get to the detector and can be measured, all the other spectra undergoes destructive interference and eliminates themselves. Bragg's Law, equation 1, gives the conditions for X-Ray beams to undergo constructive interferences.

Equation 1: $2d\sin\theta = n\lambda$

Where *d* means the distance between plains, *λ* is the wavelength, *n* is a positive integer and θ the angle.

Bragg's law interprets the crystal to have planes that reflect the X-Rays with an angle that equals the incident beam angle, as seen in figure 8. The distance between the different crystalline lattice planes determines the angle value. These angles are a "fingerprint" of the sample, every material has a unique fingerprint and it is determined by the crystal structure and the elements that form the material. d spacing is the distance between planes and it is related to the cell parameters.

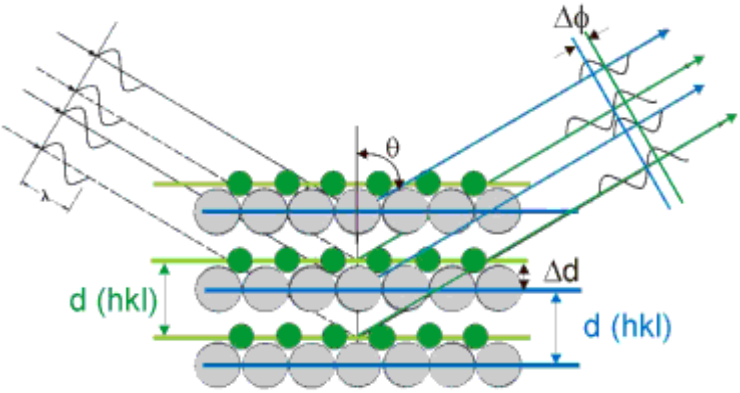

Figure 8: Bragg's Law representation

X-Ray Diffraction gives information about the number and which phases are present in our sample and the Miller indexes can be calculated from it. These Miller indexes are represented by *hkl*. All planes have their own three Miller indexes and the number they have indicate when the plane crosses the axis, the first, *h*, is for x axis, *k* is for y axis and *l* is for z axis. The more peaks there is in a XRD pattern the least symmetry has the crystal, high symmetry structures have overlapped lines so they make a single one.

XRD studies were carried out with a PNANalytical X'Pert PRO MPD Alpha1 powder diffractometer in Bragg-Brentano θ/2θ geometry of 240 millimeters of radius with a Ge (111) primary monochromator. The used radiation was Cu $K\alpha_1$ (λ = 1.5406 Å) and the work power 45 kV with 40 mA. Sample spinning at 2 revolutions per second. The diffracted beam was 0.04 radian Soller slits and was detected by X'Celerator detector with an active length of 2.122º; θ/2θ scan from 4 to 80º 2θ with step size of 0.017º and measuring time of 50 seconds. The results were interpreted with X'Pert HighScore Plus. The study was carried out on the CCiT (*Centres Científics i Tecnològics*) of the *Universitat de Barcelona*.

3.2.4. Scanning Electron Microscopy (SEM)

The Scanning Electron Microscopy studies some of the phenomena that happen when an highly voltage electron beam hits the atoms, which are the secondary electrons, which are electrons emitted from the outer shells of the atoms and have low energy, these ones give information about the morphology of the surface and the grain size. The other electrons that can be studied by SEM are the backscattered electrons, which are the electrons from the incident beam that suffer dispersion, elastic collision, when they hit the atoms under the surface. The dispersion depends on the weight of the atom, so heavier atoms disperse more than light ones and it can be used to have contrast on the image.

The electron source is a W filament or a LaB_6 crystal, with an accelerating voltage between 50 to 100 kV.

The microstructural characterization of the ceramics was made on the *Centres Científics i Tecnològics* of the *Universitat de Barcelona*, with a *JEOL JS-6510* scanning electron microscope. The samples were covered with a conductive layer of graphite carbon by evaporation.

3.2.5. Energy Dispersive X-Ray Spectroscopy (EDS)

When the electron beam from the W filament hits the sample, some inner core shell electrons are ionized and when an electron from the valence shell decays into the relaxed energy level it emits X-Rays of a precise wavelength, related to the energy gap between the shells. This X-Rays are characteristic of each element so, coupled with a Scanning Electron Microscope, the present elements on the sample can be determined.

The characterization was carried out with the same equipment that the one from SEM, using a *JEOL JS-6510* with a coupled analyzer EDS *Stereoscan 260.* Study was carried out in *Centres Científics i Tecnològics* of the *Universitat de Barcelona*.

3.2.6. Impedance Spectroscopy (IS)

The Impedance Spectroscopy studies the dielectric properties as a function of temperature and frequency, such as the dielectric losses, tan δ, which is the amount of capacitance lost in form of heat or conductivity due to crystalline defects and the relative permittivity, ε', which is the resistance to the applied electric field. This technique uses the material as a capacitor, since the impedance is the ability of a circuit to resist a flow of electrical current but it is much more complex than normal resistors. The technique is based in the application of an alternate current to a pellet of material located between two electrodes, the surface of the pellet has to be conductive so it has been covered by a thin layer of gold by plasma sputtering.

The capacitance that is measured in this technique has two components, the real part which represents the dielectric constant while the imaginary part represents the dielectric losses.

The material must be dense, with no air inside, so all the properties we measure are only from the material and have no air influence. The relative permittivity could be influenced by the porosity of the material, secondary phases, heterogeneities, crystalline defects, grain size and the material conductivity (19).

This technique also determines the dielectric anomalies related to phase transitions on the material.

The characterization was carried out with an impedance analyzer *HP 4192A* from the *Química del Estat Sòlid* group of the *Departament de Química Inorgànica I Orgànica, secció Química Inorgànica* of the *Universitat de Barcelona.*

4. OBJECTIVES

The main objective of this work is to evaluate the effect of the synthesis pathway and of doping on the functional properties of the BNT-BT based ceramics. To accomplish the main objective, specific objectives must be carried out.

- Study of the effect of ball milling in dielectric properties of BNT-BT.
- Optimizing the sintering conditions to obtain high density ceramics.
- Varying the radius and concentration of the dopant lanthanide.
- Characterization of BNT-BT based ceramics, with and without donor dopants, by solid state chemistry techniques.
- Study of the dielectric properties of the ceramics.

5. EXPERIMENTAL SECTION

Two different types of preparations have been carried out. First $0.94Bi_{0.5}Na_{0.5}TiO_3$-$0.06BaTiO_3$ (BNT-BT 0.06) ceramics were prepared. After that the $0.93Bi_{0.5}Na_{0.5}TiO_3$-$0.07BaTiO_3$ (BNT-BT 0.07) was synthetized and after three doped compositions with Lanthanides, $0.93(Bi_{0.5}Na_{0.5})TiO_3$-$0.07(Ba_{1-y}La_{2y/3})$ were y=0.15 (BNT-BT La 0.15), 0.93BNT-0.07BT La y=0.30 (BNT-BT La 0.30) and 0.93BNT-0.07BT Pr y=0.15 (BNT-BT Pr 0.15) were prepared following the same route.

The synthesis of all the BNT-BT based materials was performed through the solid state reaction route. The raw materials used for the synthesis are seen in table 1.

	Commercial reference CAS	Purity [%]	Molecular weight [g/mol]	Appearance
TiO_2	Carlo Erba 1317-70-0	≥99	79.87	White powder
Bi_2O_3	Sigma-Aldrich 1304-76-3	99.9	465.96	Yellow powder
Na_2CO_3	Sigma-Aldrich 497-19-8	≥99.5	105.99	White granulated powder
$BaCO_3$	Sigma-Aldrich 513-77-9	≥99	197.33	White powder
La_2O_3	Fluka Chemika 1312-70-0	≥99.98	325.80	White powder

Table 1: Raw materials used on BNT-BT synthesis.

The size of the reagents particles were determined (19), and was concluded that sodium carbonate has a much higher particle size on average and broader distribution. To ensure a similar average size distribution of all reagents, a previous milling with the planetary ball mill was done to Na_2CO_3. This was done to ensure similar particle distribution on the reagents since it is known that is has a big influence on the solid state reactions.

After that, a thermal treatment is made to the reagents to ensure the dehydration or to have a specific phase. Titanium dioxide is heated at 900ºC for eight hours and taken outside the muffle furnace at 900ºC so it retains its anatase structure. Bismuth oxide follows the same treatment but

at 500ºC, this one only for decarbonation. The carbonates, sodium and barium, were heated at 200ºC at the furnace all night to ensure their fully dehydration. After the thermal treatments the reactants were weighed and mixed, weighting is the most important part of the preparation because, since the synthesis has followed the solid state reaction route, the reactants have to be in stoichiometric proportion so the desired composition is obtained so the weighting has been done taking into account five significant digits.

After weighting, the mixed reagents were introduced on an yttria stabilized zirconia vessel with the help of ethanol and 1mm diameter yttria-stabilized zirconia balls in the planetary ball mill at 300 rpm for 8 hours and resuming with reverse spinning. This process was skipped on the BNT-BT 0.06 preparation and instead it was made manually with an agate mortar.

Once the milling has finished, the balls were separated and the mixture of the reagents and ethanol was dispersed with the help of a disperser working at 11000 rpm for ten minutes. This process is useful for breaking lumps and uniformly distribute in the solution. Then the mixture was placed on a hot plate until the dried product was obtained.

The resulting white powder was passed through a 90 μm mesh width sieve with the aid of a brush to obtain small and homogeneous particle size and make it easier to the reaction to take place completely. Then the product was placed on an alumina crucible for the thermal treatment.

Once the reagents were mixed and milled, each one of the composition was characterized by a thermogravimetric analysis to establish the optimal temperature for calcination. In figure 9, the TGA and DTA results are shown for the reagents used on the BNT-BT 0.07 preparation.

On the temperature studied range (25-1000ºC), the sample presents a weight loss of approximately 10%. For knowing the exact temperature when each one of the phenomena associated with weight loss take place, the derivative of thermogravimetric analysis has been represented. There are three main weight losses that are related to the endothermic processes taking place. First of all there is a loss at 90ºC, which corresponds to the water evaporation on the reagents. Then at 390ºC and 600ºC, the main weight losses are observed and correspond to the CO_2 loss due to the carbonates. Over 700ºC, there are no appreciable weight losses and changes are not appreciated on DTA so the carbonates decomposition and the formation of the perovskite BNT-BT is complete at this temperature.

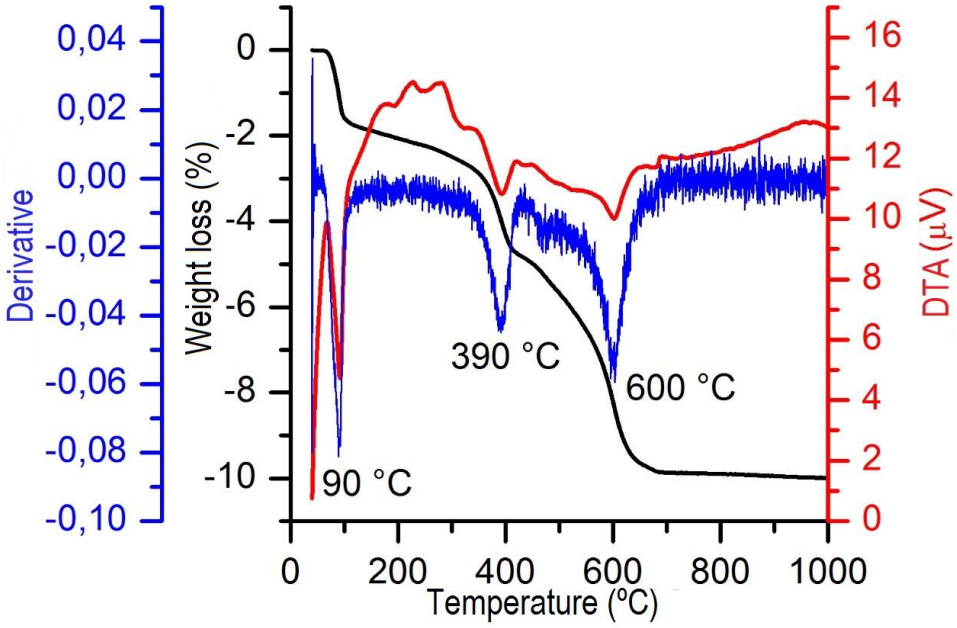

Figure 9: Thermogravimetric analysis for BNT-BT 0.07

Next the calcination was made to obtain the BNT-BT product, as it is shown on figure 10, the powder was calcined at a muffle furnace at 700ºC for two hours with a heating rate of 5ºC/min and cooling of 2ºC/min.

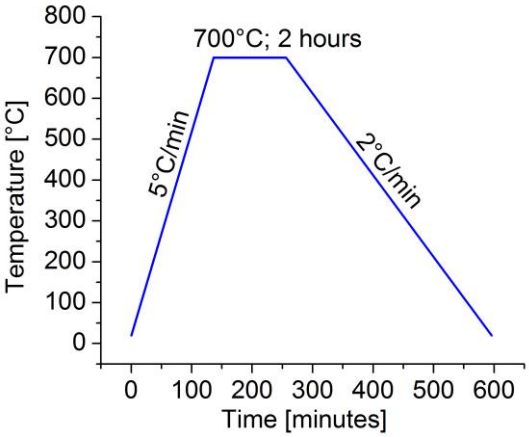

Figure 10: Calcination of the mixture of the reagents to form BNT-BT

The mixture of reagents and the calcined powder were studied by Infrared Spectroscopy (IR) in order to confirm the treatment was successful. In the IR spectra of BNT-BT, figure 11, the main focus on the powder before calcination is the ~1425cm^{-1} band which corresponds to the asymmetric stretching of C-O bonds of the carbonate anions and also the outer plane deformation of CO_3^{2-} which is around 850cm^{-1} and this bands are not found in the calcined product. The other important bands are the Ti-O bonds which can be found at 630-680cm^{-1}, these are the bands that should be found on the product due to the TiO_6 octahedrons.

Finding the Ti-O bonds confirms the formation of the perovskite structure of the BNT-BT after the calcination at 700ºC and not finding the C-O bonds confirms the total decomposition of the carbonates.

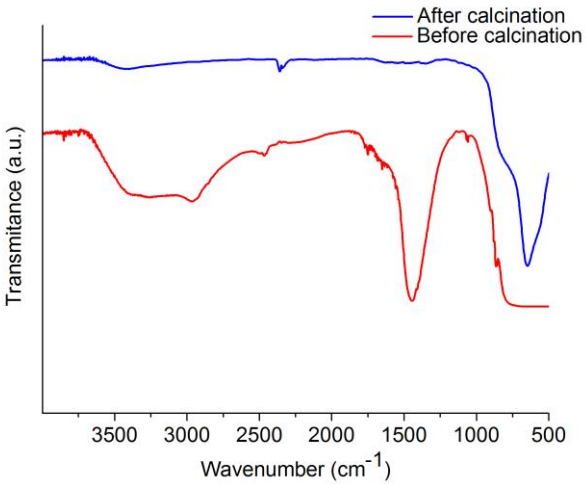

Figure 11: FT-IR spectra of the mixture of reagents versus the calcined powder of BNT-BT.

As it can be appreciated, these results show that the treatment at 700ºC for 2 hours is effective as for the decomposition of carbonates and the formation of the perovskite structure of BNT-BT.

The powder calcined at 700ºC, BNT-BT 0.06, was analyzed using X-Ray Diffraction to ensure the lack of impurities and assure the process was optimum. The XRD pattern of the powder was obtained and, by comparison with the Powder Diffraction File (PDF) patterns of the International Centre for Diffraction Data (ICDD) database, a BNT-BT phase with perovskite structure was found as can be seen in figure 12 including a mixture of reactants, since the milling was made manually without using the planetary ball mill (20). We can conclude that a 700ºC thermal treatment without using the planetary ball mill is not enough to obtain the unique phase of BNT-BT.

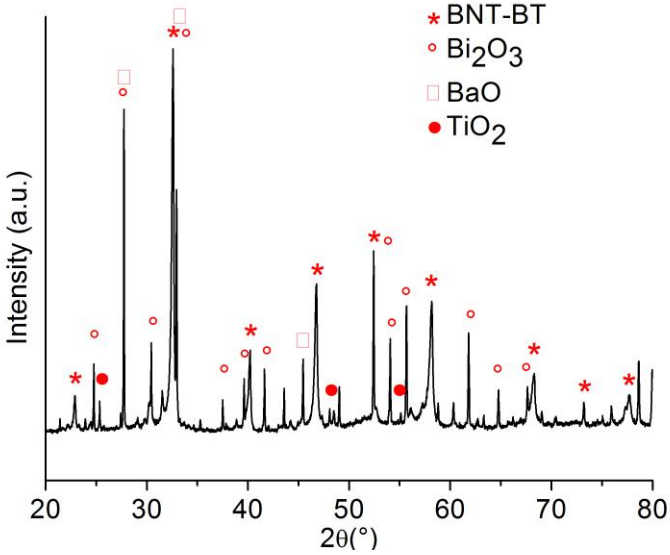

Figure 12: XRD of calcined powder of BNT-BT 0.06 without planetary ball milling

Then the XRD of the calcined powder at 700ºC of BNT-BT 0.07. As it can be seen in figure 13, all peaks on the calcined powder correspond to BNT-BT so it can be said that the planetary ball mill, hence the particle homogeneity and size, affects the fulfillment of the reaction. Also, a unique perovskite phase has been found for BNT-BT 0.07.

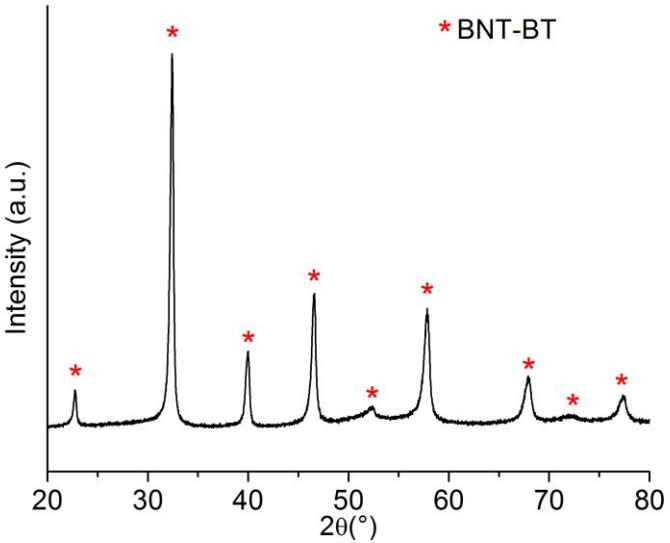

Figure 13: XRD of calcined powder of BNT-BT 0.07 with planetary ball milling

Also, studies of XRD of the calcined powders of BNT-BT La 0.15; BNT-BT La 0.30 and BNT-BT Pr 0.15 were made, all of them showing the same pattern, a unique phase of perovskite.

Once calcined, the product has already been formed but for reducing particle size so we achieve high density the powder is once again passed through a 90 μm mesh width sieve and then milled on the planetary ball mill with the yttria-stabilized zirconia balls. Then binder PARALOID-67 (Rohm and Hass) was added to aid the densification and the solution was dispersed at 11000 rpm. Then the solution was placed on a hot plate and completely dried on the furnace for all the night. After that it was passed again through a 90 μm mesh width sieve.

The pellets were formed with a uniaxial press applying a pressure of 700 MPa. Three pellets were formed per each composition and sintering temperature. One is used for X-Ray Diffraction so, once sintered, it crushed into fine powder for its analysis and the other ones were used for SEM and IS.

For the sintering, the pellets were deposited over a platinum film, were covered with sacrifice powder of the same composition and were covered by another platinum film to prevent the volatilization of the present elements, mainly bismuth and sodium.

Pellets were introduced at a tubular furnace at three different sintering temperatures, 1100ºC, 1150ºC and 1200ºC, following the scheme on figure 14. The first stop at 700ºC for two hours is to ensure the complete evaporation of the binder and then the temperature rises at 0.5ºC/min to the sintering temperature and it remains at the same temperature for two hours to cool down at 2ºC/min to room temperature.

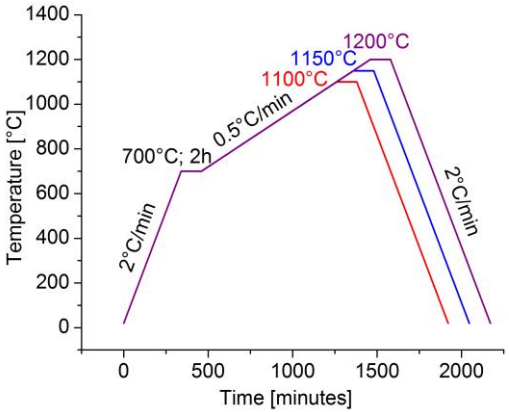

Figure 14: Sintering ramps done to the pellets of BNT-BT.

After the sintering, the 0.4 g pellet was crushed into powder on an agate mortar for the posterior XRD analysis. The other two 0.2 g pellets were studied to see which has the higher density. For the density calculations two measurements were done, one with the digital caliper and the other one using Archimedes method with the help of the analytical balance with the densities measurement set. Then the denser one, arriving at relative densities over 97-98% determined from the maximum density of the BNT-BT pattern, 5.9 g/cm^3, was polished until almost 1 mm thickness. The results of the density studies are shown in table 2.

Composition	Density [% on 5.9 g/cm^3] on Arquimedes method					
Sintering temperature	1100ºC		1150ºC		1200ºC	
BNT-BT 0.06	91	86	90	89	92	91
BNT-BT 0.07	96	96	98	98	98	97
BNT-BT La 0.15	98	97	98	98	98	96
BNT-BT La 0.30	97	94	98	97	98	98
BNT-BT Pr 0.15	99	96	96	96	98	94

Table 2: Density studies of the sintered pellets

6. RESULTS AND DISCUSSION

6.1. X-RAY DIFFRACTION (XRD)

XRD studies were made to the sintered pellets to obtain information about the phase and the crystalline structure. The X-Ray Diffraction pattern of BNT-BT used for the study was PDF-01-089-3109. Studies on the sintered lanthanides doped BNT-BT have been carried out also to confirm the unique perovskite phase and determine its crystalline structure.

The results were interpreted taking into account that BNT presents a rhombohedric structure at room temperature (21) and BT presents a tetragonal structure at room temperature (22). On the MPB both structures are found.

First, the BNT-BT 0.06 sintered pellets were studied. The results are shown in figure 15 a-b.

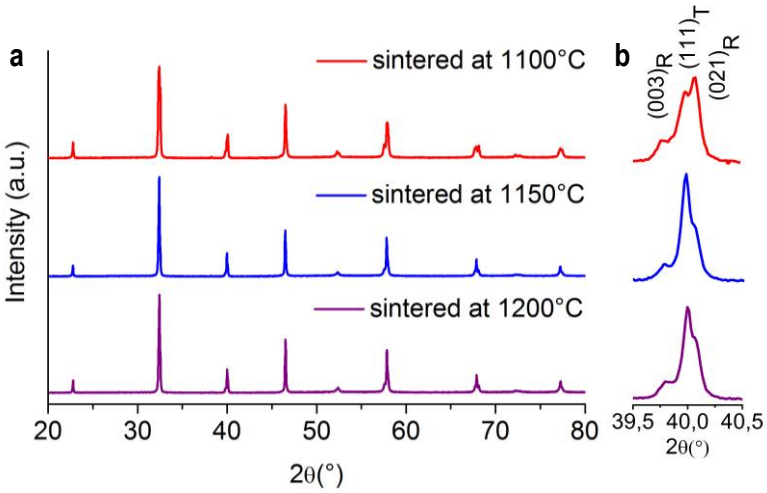

Figure 15: a. BNT-BT 0.06 XRD study of sintered pellets at different temperatures, b. zoomed region of 40º

On figure 15a., a unique phase of perovskite is observed. On figure 15b., it can be seen a coexistence of crystalline structures and it can be appreciated the coexistence of the tetragonal, the (111) reflection on the 40º region, and rhombohedric structure, the reflections (003) and (021) at the 40º region, it can also be observed a tendency to a rise on the tetragonal structure and drop of rhombohedral structure as the sintering temperature rises.

After the BNT-BT 0.06 XRD study, it was also performed on the BNT-BT 0.07, the results are shown in figure 16 a-b.

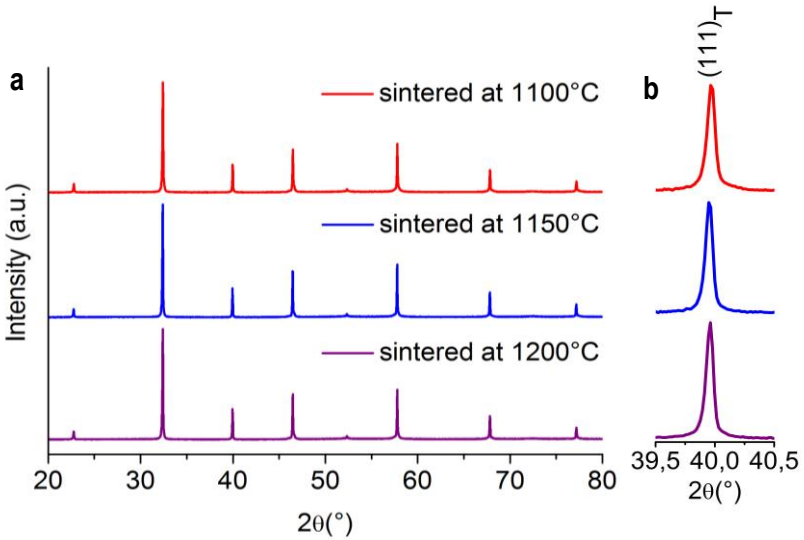

Figure 16: a. BNT-BT 0.07 XRD study of sintered pellets at different temperatures, b. zoomed region of 40º

On figure 16a., corresponding to BNT-BT 0.07, it is shown also a unique perovskite phase. On figure 16b., only one reflection (111) corresponding to a tetragonal crystalline structure is observed. So as it should still be some crystalline structures coexistence because the maximums at the 40º region are asymmetric searching was done on some articles, there an article of L. Chen *et al.* (23) that has performed a XRD study with a synchrotron and they found that inside these maximums of the tetragonal structure lie the maximums of rhombohedric structure, the theoretical coexistence is has high as a 48.4% of rhombohedric structure and 51.6% of tetragonal structure (19), these results were obtained by Rietveld analysis on the *Química del Estat Sòlid* group of the department of *Química Inorgànica i Orgànica, secció de Química Inorgànica* of the *Universitat de Barcelona*.

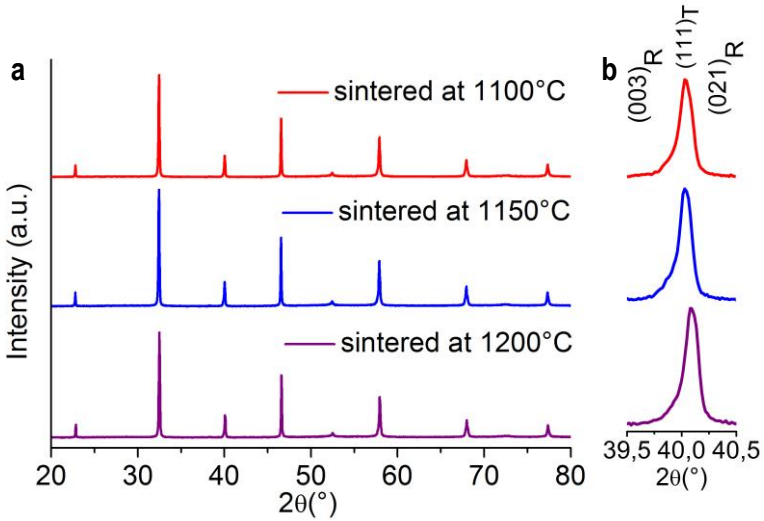

Figure 17: a. BNT-BT La 0.15 XRD study of sintered pellets at different temperature,

b. zoomed region of 40º

The diffraction pattern, figure 17a., shows the formation of a unique phase of perovskite in all the sintered pellets of BNT-BT La 0.15. In the more detailed study on the 40º region, figure 17b., it is shown a rhombohedric structure with coexistence of tetragonal with,the reflections (003) and (021) belonging to rhombohedric and (111) to tetragonal.

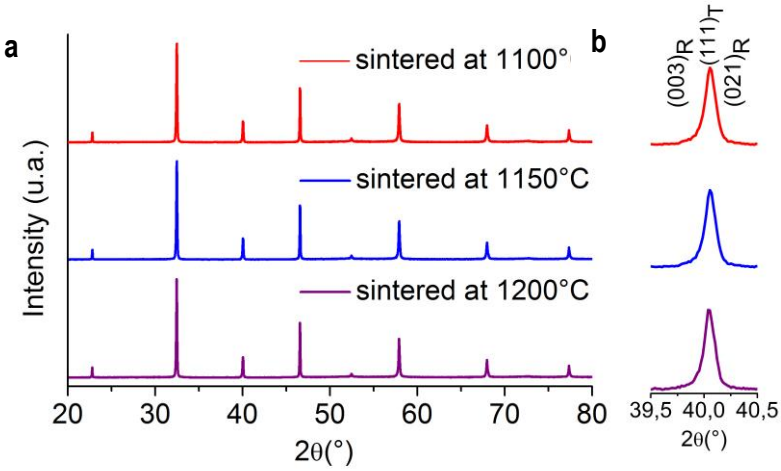

Figure 18: a. BNT-BT La 0.30 XRD study of sintered pellets at different T, b. zoomed region of 40º

The diffraction pattern, figure 18a., BNT-BT La 0.30, shows the formation of a unique phase of perovskite in all the sintered pellets. In the more detailed study, figure 18 b., on 40º region, it is shown a rhombohedric structure with coexistence of tetragonal with the reflections (003) and (021) belonging to rhombohedric and (111) to tetragonal since the maximum is not symmetric.

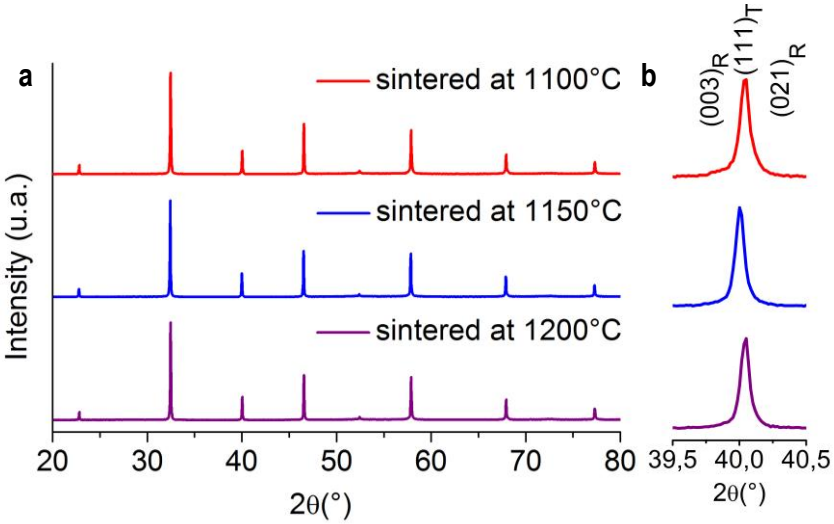

Figure 19: a. BNT-BT Pr 0.15 XRD study of sintered pellets at different temperatures,

b. zoomed region of 40º

The diffraction pattern, figure 19a., BNT-BT Pr 0.15, shows the formation of a unique phase of perovskite in all the sintered pellets. In the more detailed study, figure 19b., on 40º region, it is shown a rhombohedric structure with coexistence of tetragonal with the reflections (003) and (021) belonging to rhombohedric and (111) to tetragonal since the maximum is not symmetric.

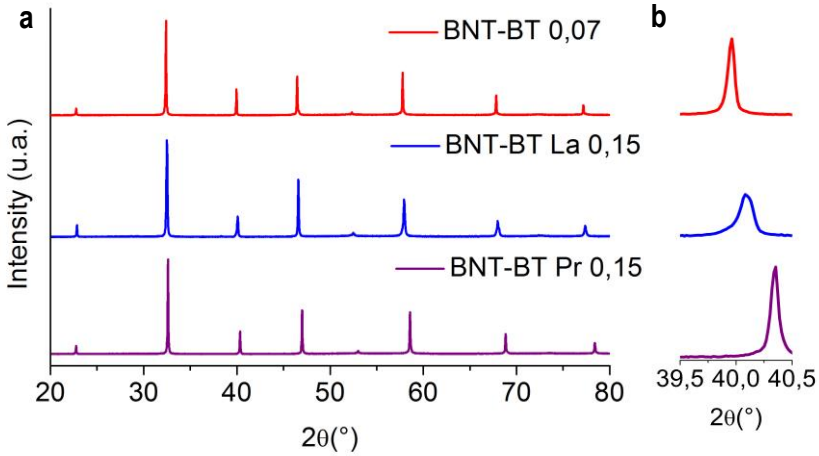

Figure 20: a. Non-doped BNT-BT 0.07, BNT-BT La 0.15 and BNT-BT Pr 0.15. b. zoomed region of 40º

The diffraction pattern, figure 20a, shows the formation of a unique phase of perovskite in the three different compositions. In a more detailed study, figure 20b, on the 40º region, it is shown a displacement of the maximum to greater angles, meaning the reduction of the unit cell volume because of the incorporation of lanthanides of smaller radius on the barium titanate structure, taking in account that Ba^{2+} has a r = 1.35 Å, La^{3+} r = 1.22 Å and Pr^{3+} r = 1.06 Å, all have coordination number 12, that confirms the introduction of the lanthanides on the BNT-BT structure (24).

6.2. SCANNING ELECTRON MICROSCOPY – ENERGY DISPERSIVE X-RAY SPECTROSCOPY (SEM/EDS)

The Scanning Electron Microscopy micrographs of the BNT-BT 0.07 at different sintering temperatures are shown in figures 21 a-c, being the temperatures 1100ºC, 1150ºC and 1200ºC. An increasing on the grain size is related to a higher sintering temperature, almost doubling size at each sintering temperature. All images have been take at 3000 magnifications.

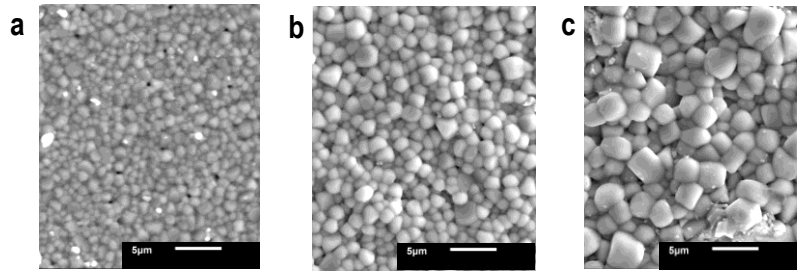

Figure 21: SEM images corresponding to the secondary electrons image. a. BNT-BT 0.07 sintered at 1100ºC, b. sintered at 1150ºC and c. sintered at 1200ºC.

The scanning electron microscopy micrographs of all the BNT-BT prepared are shown on figure 22 a-d. The images show polycrystalline structure of the ceramics with a compact microstructure. The BNT-BT 0.06, figure 22b, shows polyhedral shaped grains, bigger in size than on the BNT-BT 0.07, figure 22a, composition which has cuboidal shaped grains. The lanthanum composition, figure 22c and 22d, shows cuboidal grains.

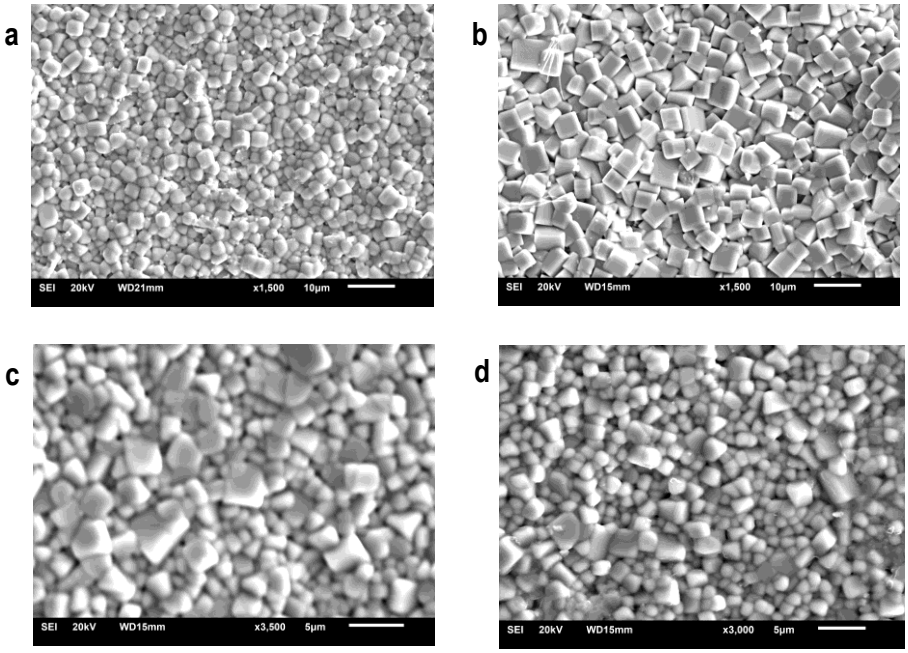

Figure 22: Micrograph of ceramic materials a. BNT-BT 0.07, b. BNT-BT 0.06,

c. BNT-BT La 0.15 and d. BNT-BT La 0.30

Grain size distribution of the prepared ceramics was analyzed by Fullman intersection method (25). A minimum of 300 grains per image was used on the analysis. The results are shown on table 3.

Composition	d_{50} (μm)
BNT-BT 0.07 sintered at 1100ºC	1.43±0.15
BNT-BT 0.07 sintered at 1150ºC	1.75±0.14
BNT-BT 0.07 sintered at 1200ºC	2.97±0.36
BNT-BT 0.06 sintered at 1200ºC	4.66±0.52
BNT-BT La 0.15 sintered at 1200ºC	2.41±0.12
BNT-BT La 0.30 sintered at 1200ºC	1.99±0.18

Table 3: Grain size of BNT-BT for the prepared compositions.

An increase on the barium titanate quantity produces a reduction of the grain size, as it can be observed from the maximum on grain size by the BNT-BT 0.06 since the barium titanate causes inhibition of the grain growth, there is also a contribution of the ball milling process. Also an increase on the sintering temperature increases grain size. An increase on the quantity of lanthanum decreases grain size, a possible explanation to this phenomena could be that an excess of La^{3+} cations near the grain boundaries could reduce its mobility, reducing mass transport and hence it's growing during the sintering. (19).

All the ceramics have regions of different morphology, these regions were analyzed by energy dispersive spectroscopy (EDS), figures 23c. and 23d. The images are shown in figure 23 SEI (secondary electrons image) and BSE (backscattered secondary electrons), 23a. and b.

They present two differenced morphologic regions, these regions were also analyzed by EDS, figure 23c. and d. The bright region analysis shows a majority of bismuth, sodium, titanium, BNT grains, and the dark region a majority of barium and titanium, BT grains. It can be considered BNT-BT as a matrix of $(Bi_{0.5}Na_{0.5})TiO_3$ with grains of $BaTiO_3$.

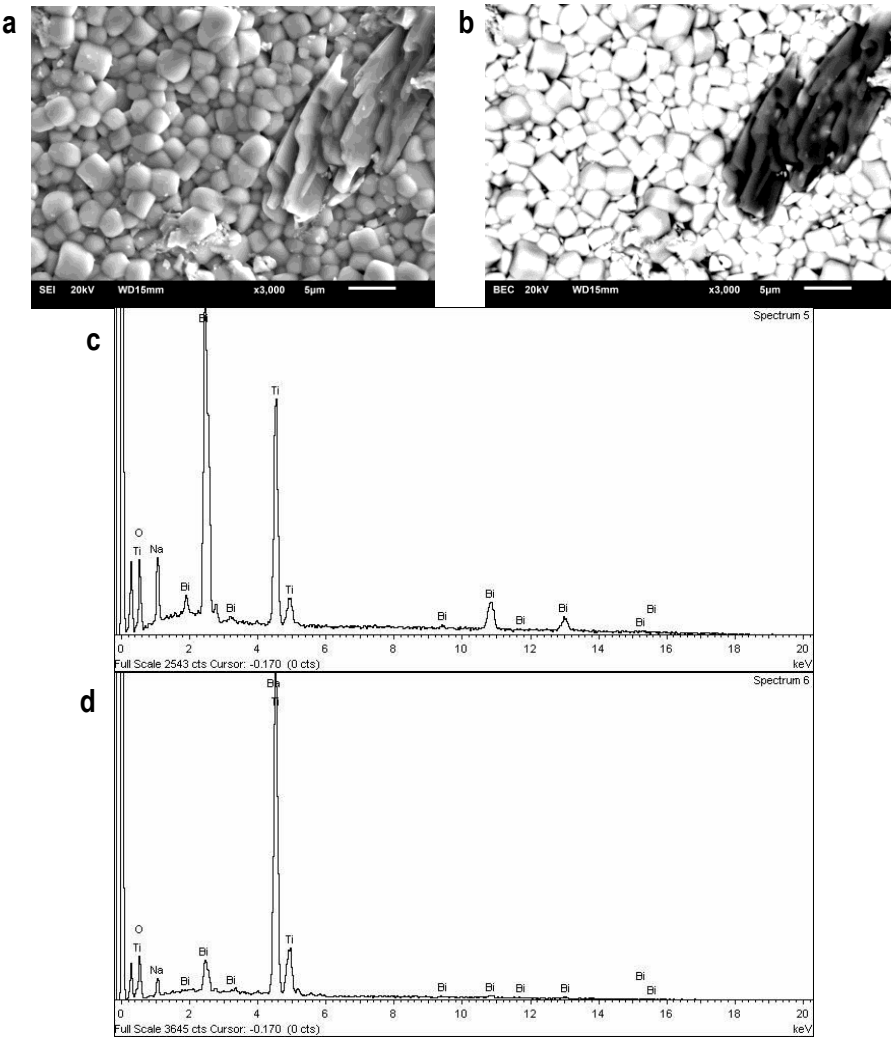

Figure 23: a. SEI and b. BSE images of BNT-BT 0.07 sintered at 1200ºC and EDS analysis for c. BNT and d. BT grains.

Lanthanum α band is shown at 4.650 keV, same as titanium and barium, reason why it is not represented on EDS graphic, figure 24c. and 24d. and also because the low content on the composition.

The addition of lanthanum promotes the growing of barium titanate grains , figure 24a. and 25a., while bismuth sodium titanate grains show similar size in both compositions. Barium titanate grains on lanthanum compositions show polyhedral shape, although being smaller than the non-doped composition and bismuth sodium titanate grains show smaller size than the BNT-BT 0.07 composition grains.

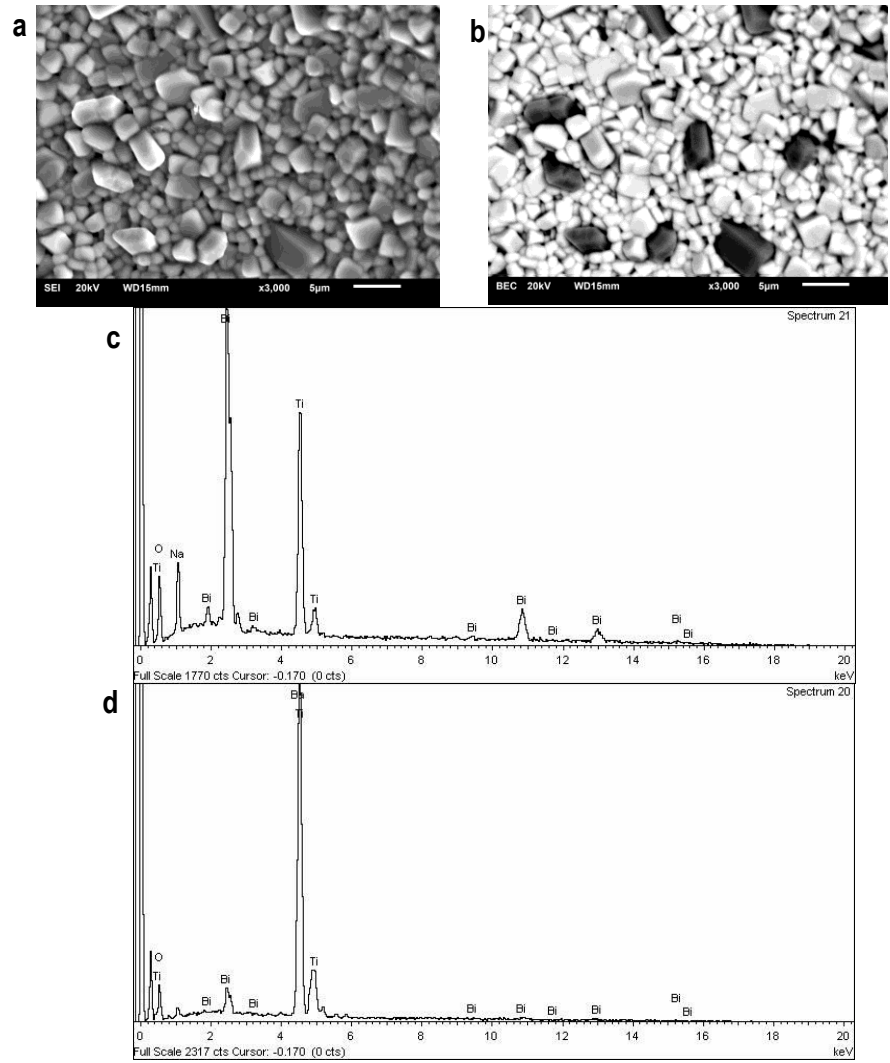

Figure 24: Above a. SEI and b. BSE images of BNT-BT La 0.15, underneath c. EDS of BNT and d. EDS of BT

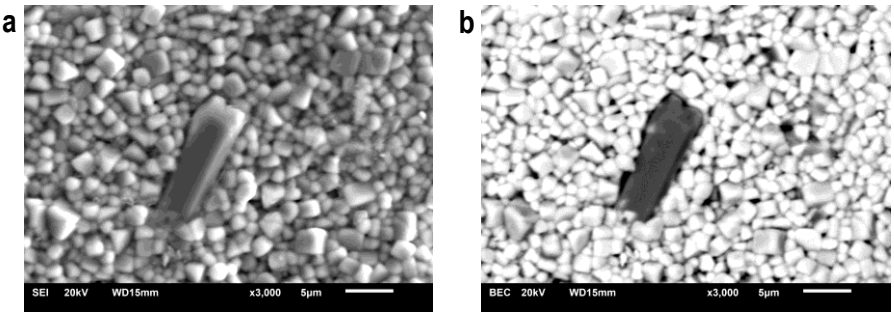

Figure 25: Above a. SEI and b. BSE images of BNT-BT La 0,30.

6.3. IMPEDANCE ANALYSIS (IS)

For studying the characteristics of the transitions of BNT-BT, the relative permittivity as a function of the temperature at different frequencies was measured (1 kHz – 1000 kHz). In figure 26 the results of the study for BNT-BT 0.07 are shown, all the compositions prepared show the same behavior.

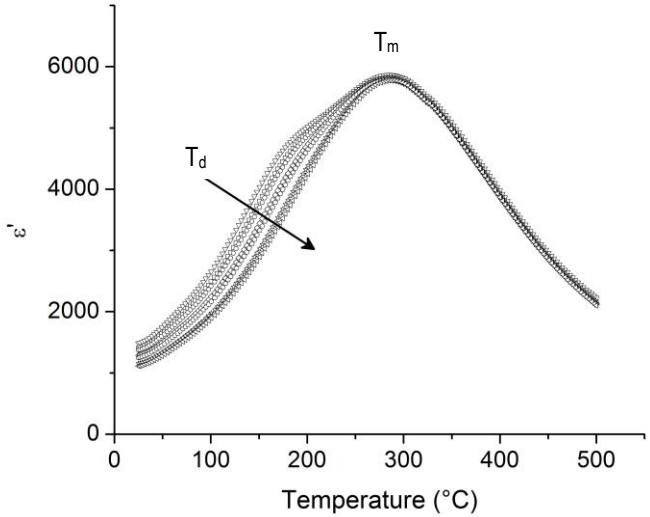

Figure 26: Dependency of the relative permittivity with temperature at different frequencies for BNT-BT 0.07.

The results show clearly the dependence of the permittivity with the frequency round and before T_d, corresponding to ferroelectric – antiferroelectric phase transition, and is a typical behavior of phase transition relaxor type. For the maximum of permittivity related to the antiferroelectric – paraelectric transition (T_m), is wide and independent of frequency, typical behavior of a diffuse phase transition. First anomaly is related to the ferroelectric-antiferroelectric transition which is known as the depolarization temperature (T_d) and occurs near 150ºC and the second anomaly, related to the antiferroelectric-paraelectric phase transition (T_m), occurs between 250ºC and 300ºC, where the relative permittivity reaches its maximum value.

As the objective of this preparation was to determine whether it was useful or not the ball milling process, the results were compared to the results obtained with the same composition with ball milling process by Elena Cerdeiras in her PhD, (19), these results are shown in table 3.

BNT-BT 0.06 sintered at 1200ºC	ε' at room T at 1 kHz	Maximum ε' (at T_m) at 1 kHz	Dielectric losses (tan δ at room T at 1 kHz
With ball milling process	1673	6119	0,1238
Without ball milling process	1013	2575	0,0808

Table 3: Comparison of BNT-BT 0.06 with and without ball milling process

The results show that ball milling process, hence reducing particle size, affects positively on the values of relative permittivity at room temperature and at the maximum value of relative permittivity (at T_m). At room temperature, and at all temperatures, the values of dielectric losses are a little bit lower at the BNT-BT 0.06 without ball milling process but the value of the BNT-BT 0.06 with ball milling process are still very low so ball milling process affects positively at the properties of BNT-BT so it is correct to apply it at all the compositions.

Figure 27 a-b., show the relative permittivity and dielectric losses at 1 kHz versus temperature of BNT-BT 0.06 sintered at different temperatures. Results show an increase in relative permittivity with the sintering temperature and the maximum is shown at 1200ºC, hence being the best sintering temperature for BNT-BT 0.06 ceramics. Typical dielectric anomalies are clearly shown.

The ceramic sintered at 1200ºC exhibits lower values of losses. After the second transition both sintering temperatures rise their values abruptly.

The broadening of the antiferroelectric - paraelectric phase transition is a typical behavior of diffuse phase transition. The ferroelectric – antiferroelectric transition is a relaxor phase transition as it was said before. The marked diffuse phase transition may occurs because of the disordering of A-site cations caused by the addition of Na^+, Bi^{3+} and Ba^{2+} cations which are randomly distributed on the perovskite structure (26).

Results of the 1100ºC sintered ceramics are not shown since they could not be carried out successfully.

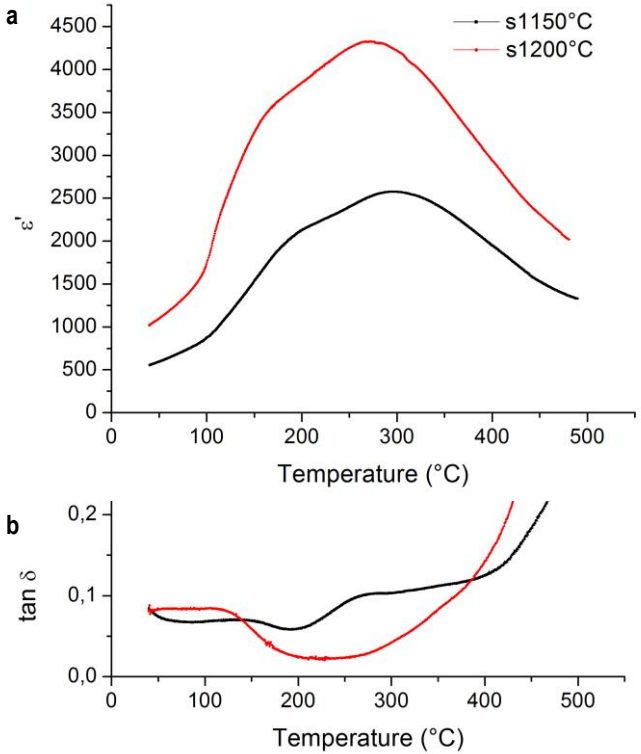

Figure 27: a. Dependence of relative permittivity (ε') with temperature for BNT-BT 0.06 and b. evolution of the dielectric losses (tan δ) with temperature for BNT-BT 0.06 ceramics

On figure 28 a-b., dependence with frequency is shown, showing stable permittivity, figure 28 a., for all three sintering temperatures and being the 1200ºC sintering temperature the best for

the relative permittivity values. For the dielectric losses, figure 28 b., the 1200ºC sintering temperature shows lower values at first and they stabilize and at high frequencies are the highest while for the other two sintering temperatures the values descend as the frequency rises.

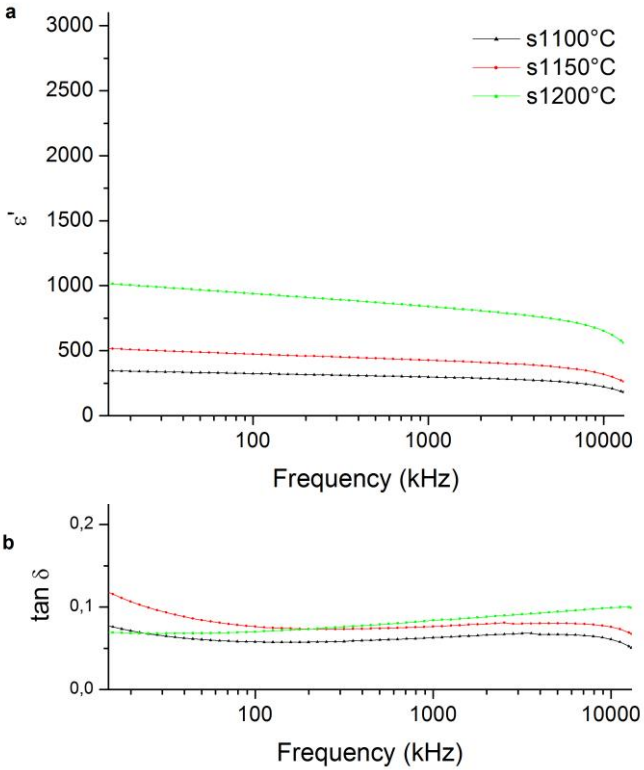

Figure 28: a. Dependence of relative permittivity (ε') with frequency and

b. evolution of the dielectric losses (tan δ) with frequency for BNT-BT 0.06 ceramics

In figure 29 the results of relative permittivity and dielectric losses at 1 kHz depending on temperature of BNT-BT 0.07 sintered at different temperatures are shown. Results show an

increase in relative permittivity with the sintering temperature and the maximum is shown at 1150ºC, hence being the best sintering temperature for non-doped BNT-BT 0.07 ceramics.

The values of permittivity and dielectric losses show an improvement at 1150ºC, also at 1200ºC values are good and near the values of 1150ºC but at 1100ºC they shown poor values of permittivity and high dielectric losses, being 1150ºC the best sintering temperature for BNT-BT 0.07.

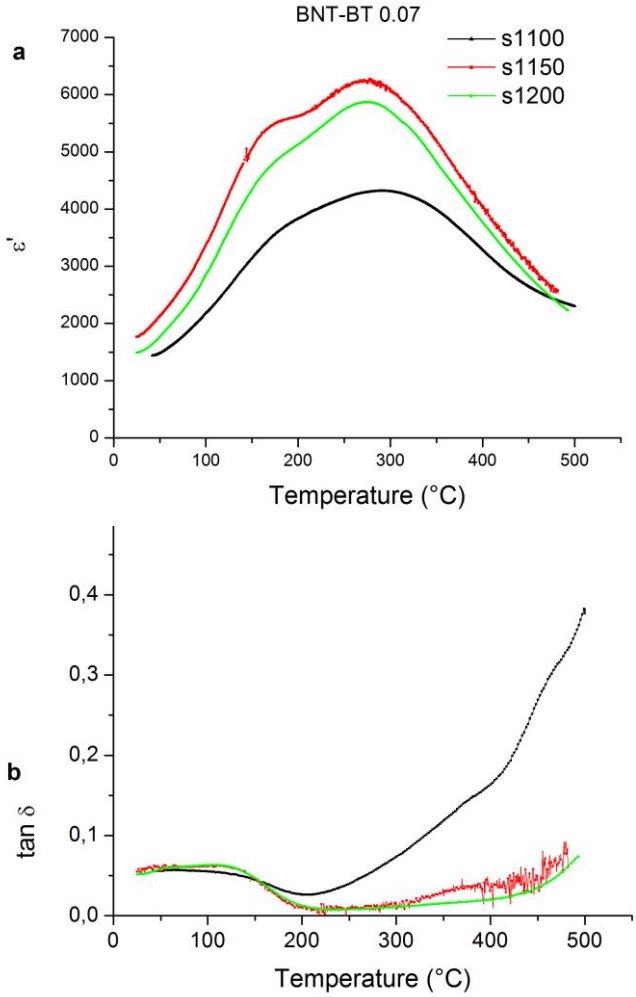

Figure 29: a. Dependence of relative permittivity (ε') with temperature and

b. evolution of the dielectric losses (tan δ) with temperature for BNT-BT 0.07 ceramic

For further study on the transitions characteristics, varying frequency studies were also carried out. In figure 30 a-b. the results of relative permittivity and dielectric losses at room temperature depending on the frequency for BNT-BT 0.07 sintered at different temperatures are shown. Frequency varied from 0.5 to 13000 kHz. The same results are shown on frequency dependent relative permittivity and dielectric losses, all values being similar. The study shows a reducing of relative permittivity at the frequency rises and an increase on the dielectric losses.

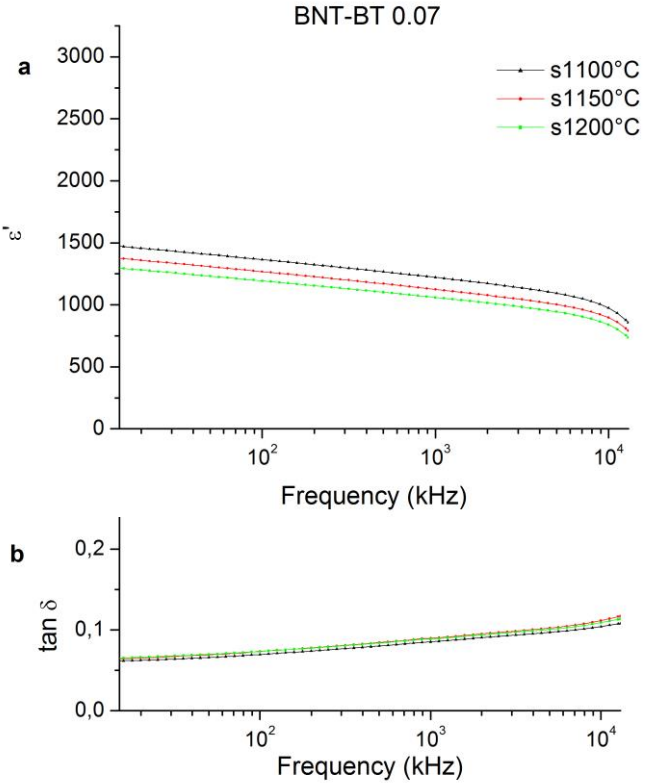

Figure 30: a. Dependence of relative permittivity (ε') with frequency and b. evolution of the dielectric losses (tan δ) with frequency for BNT-BT 0.07 ceramics

The results of relative permittivity and dielectric losses at 1 kHz depending on temperature, figure 31 a-b., of BNT-BT La 0.15 sintered at different temperatures show an increase on the relative permittivity with the increasing of the sintering temperature, being the best sintering temperature 1200ºC. Dielectric losses go in accordance with the relative permittivity, being the

1200ºC sintered composition the material with lower dielectric losses but all of them are low. The results also show the dielectric anomalies related to BNT-BT ceramics.

On the dielectric losses graphic, figure 31 b., low values of dielectric losses are shown, this losses fall down after the ferroelectric-antiferroelectric phase transition and rise after the antiferroelectric - paraelectric phase transition.

Antiferroelectric - paraelectric phase transition on T_m is widely broad on all three ceramics, typical behavior of a diffuse phase transition.

When comparing the best sintering temperatures for relative permittivity and dielectric losses, based on the higher values of relative permittivity depending on temperature and frequency, for non-doped BNT-BT 0.07 and the ceramics doped with Lanthanum on figure 31 a-b. and 32 a-b., a drop on the values of relative permittivity both depending on temperature and on frequency is found in doped ceramics, although the dielectric losses depending on temperature and frequency are lower on the doped ceramics, especially depending on frequency. Also the ferroelectric - antiferroelectric transition temperature is lower on doped ceramics than for the non-doped ceramics, figure 31a., but there is no dependence on the quantity of Lanthanum on the temperature because the transition temperature for the higher doper ceramic, BNT-BT La 0.30, is higher than for the lower doped ceramic, BNT-BT La 0.15.

The dielectric losses on the BNT-BT La 0.30 ceramic seems to rise to high values of dielectric losses after the antiferroelectric - paraelectric transition.

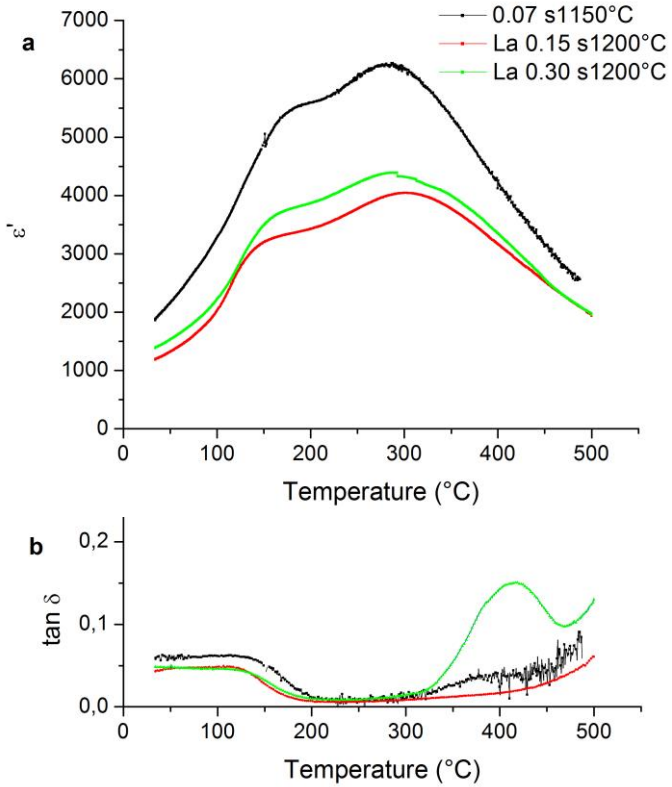

Figure 31: a. Dependence of relative permittivity (ε') with temperature b. evolution of the dielectric losses (tan δ) with temperature for BNT-BT La 0.15, BNT-BT La 0.30 and BNT-BT 0.07 ceramics at the same frequency (1 kHz).

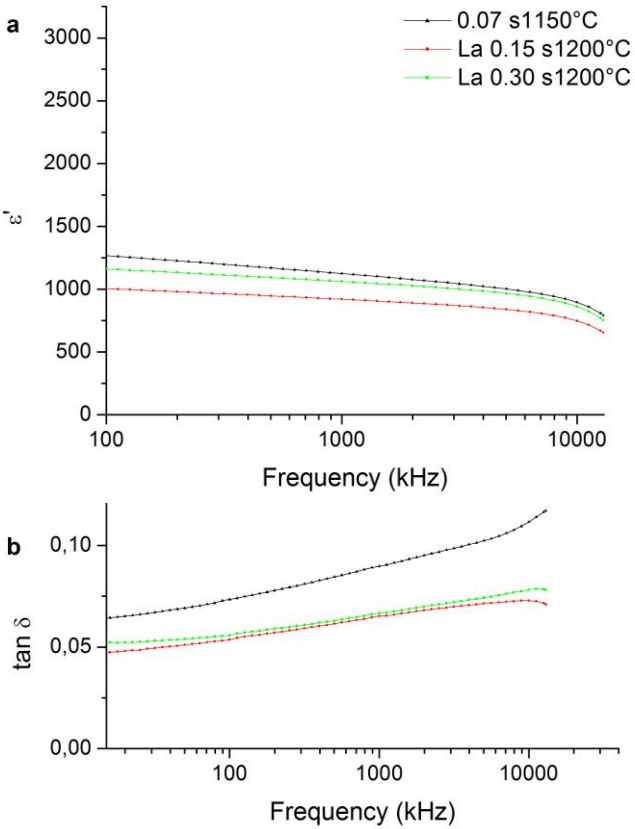

Figure 32: a. Dependence of relative permittivity (ε') with frequency b. evolution of the dielectric losses (tan δ) with frequency for BNT-BT La 0.15, BNT-BT 0.30 and BNT-BT 0.07 ceramics at the same frequency (1 kHz)

Also, the non-doped BNT-BT 0.07 was compared to the different doped compositions of the same quantity of lanthanide, BNT-BT La 0.15 and BNT-BT Pr 0.15 on figure 33 a-b. It can be observed that, even changing the doping element, the properties related to the maximum of permittivity are still lower than the non-doped composition values, even though Praseodymium shows higher values of permittivity than Lanthanum, figure 33a. The dielectric losses, figure 33b., are low in all three ceramics and quite similar between them.

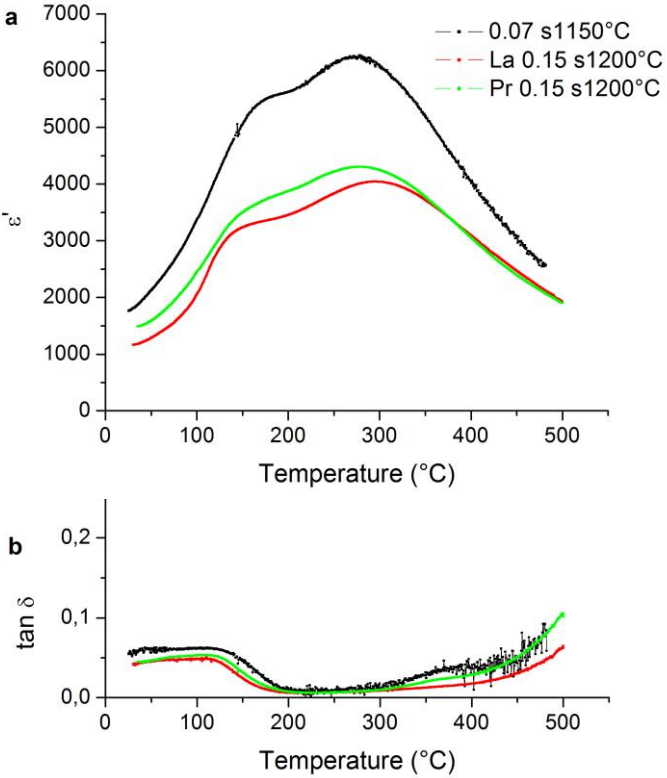

Figure 33: a. Dependence of relative permittivity (ε') with temperature b. evolution of the dielectric losses (tan δ) with temperature for BNT-BT La 0.15, BNT-BT Pr 0.15 and BNT-BT 0.07 ceramics at the same frequency (1 kHz)

The results of the relative permittivity and dielectric losses dependent on frequency, figure 34 a-b., show that the best composition would be the Praseodymium doped composition, reaching higher values of relative permittivity than the non-doped composition and also having less dielectric losses than he non-doped ceramic.

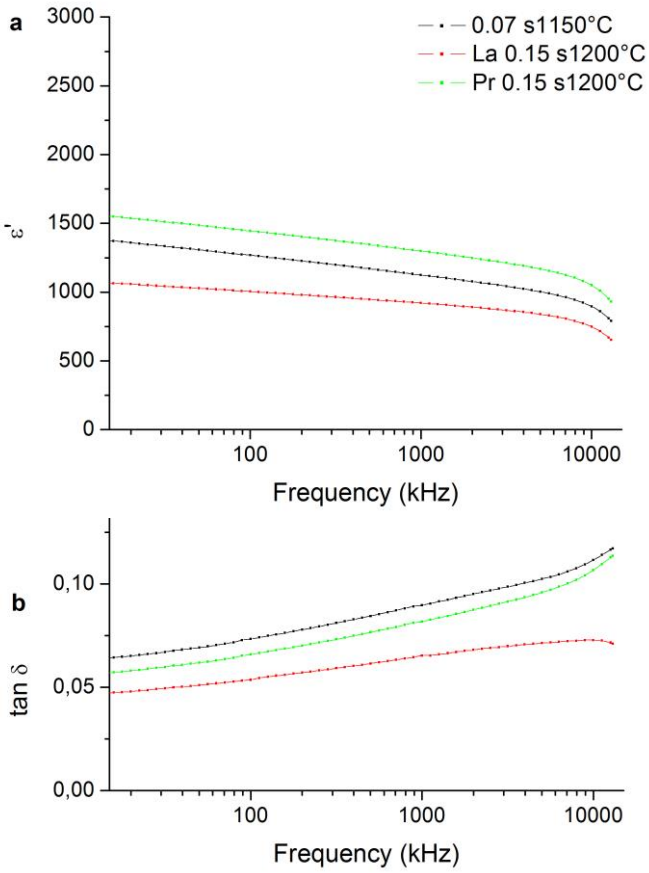

Figure 34: a. Dependence of relative permittivity (ε') with frequency b. evolution of the dielectric losses (tan δ) with frequency for BNT-BT La 0.15, BNT-BT Pr 0.15 and BNT-BT 0.07 ceramics at the same frequency (1 kHz)

7. CONCLUSIONS

The main objective of this work was to evaluate the effect of the synthesis route and doping on the functional properties of BNT-BT based ceramics. From the results obtained in this work the following conclusions have been proposed.

It has been observed the importance of following the solid state reaction by the different characterization techniques of the solid state chemistry. This has let us establish the synthesis pathway by planetary ball milling and optimizing the sintering conditions to obtain high density ceramics.

BNT-BT based ceramics have been obtained. In all cases, these ceramics present perovskite unique and rhombohedric and tetragonal phases coexist so these ceramics are in the morphotropic phase boundary. Using Scanning Electron Microscopy a BNT matrix with grains of BT has been observed on the ceramics.

By doping BNT-BT with lanthanides a unique phase of perovskite has been stabilized. The displacement of the XRD maximums to higher angles is related to the incorporation of cations of lower radius and vacancies, confirming that the dopants have been introduced in the BNT-BT structure. It has been observed that the introduction of lanthanides, donor dopants, on the A position of the perovskite, generates cationic vacancies that influence on the dielectric properties of the material. A morphologic variation of the barium titanate grains when doping with Lanthanum has been observed, which let us propose that the Lanthanum has been introduced on the barium titanate structure. It has also been observed that varying the lanthanide, Praseodymium instead of Lanthanum, presents better frequency dependent behavior related to relative permittivity and dielectric losses.

The results obtained in this study let us determine that the synthesis pathway and the doping allow the modulation of the dielectric properties of the BNT-BT based ceramics in the morphotropic phase boundary.

8. REFERENCES AND NOTES

1. Haertling G.H. Ferroelectric ceramics: history and technology. J Am Ceram Soc. 1999;82(4):797–818.
2. Brewster D. Observations on the Pyro-Electricity of Minerals. Edinburgh J Sci. Edinburgh ;London: William Blackwood ;T. Cadell; 1824;1:206–15.
3. Curie J, Ph P.C. Phénomènes électriques des cristaux hémièdres à faces inclinées Jacques Curie , Pierre Curie, 1882;
4. Morgan Technical Ceramics. Introduction. Piezoelectric Ceram Prop Appl. 2013;
5. Jaffe B., Roth R.S., Marzullo S. Piezoelectric Properties of Lead Zirconate-Lead Titanate Solid-Solution Ceramics. J Appl Phys. American Institute of Physics; 1954 Jun;25(6):809–10.
6. Cady W.G. Piezoelectricity : an introduction to the theory and applications of electromechanical phenomena in crystals. McGraw-Hill; 1946.
7. Morgan Technical Ceramics. Physical Basis. Piezoelectric Ceram Prop Appl. 2013;1–12.
8. Norman Lockyer. Nature - Google Libros. Nature. 1873
9. Glazer A.M., IUCr. The classification of tilted octahedra in perovskites. Acta Crystallogr Sect B Struct Crystallogr Cryst Chem. International Union of Crystallography; 1972 Nov 15;28(11):3384–92.
10. Glazer A.M. Simple ways of determining perovskite structures. Acta Crystallogr Sect A. 1975;31(6):756–62.
11. Jaffe H. Piezoelectric Ceramics. J Am Ceram Soc. Blackwell Publishing Ltd; 1958 Nov;41(11):494–8.
12. Noheda B., Cox D.E., Shirane G., Gonzalo J.A., Cross L.E., Park S.E. A monoclinic ferroelectric phase in the Pb(Zr1−xTix)O3 solid solution.. American Institute of Physics; 1999
13. Zvirgzds J.A., Kapostin P.P., Zvirgzde J.V., Kruzina T.V. X-ray study of phase transitions in efrroelectric $Na_{0.5}Bi_{0.5}TiO_3$. Ferroelectrics. Taylor & Francis Group ; 1982 May 15;40(1):75–7.
14. Hagiyev M.S., Ismailzade I.H., Abiyev A.K. Pyroelectric properties of ($Na_{½}Bi_{½}$)TiO_3 ceramics. Ferroelectrics. Taylor & Francis Group ; 1984 Apr 15 ;56(1):215–7.
15. Suchanicz J., Roleder K., Kania A., Hańaderek J. Electrostrictive strain and pyroeffect in the region of phase coexistence in $Na_{0.5}Bi_{0.5}TiO_3$. Ferroelectrics. Taylor & Francis Group ; 1988 Jan;77(1):107–10.
16. Hiruma Y., Nagata H., Takenaka T. Thermal depoling process and piezoelectric properties of bismuth sodium titanate ceramics. J Appl Phys. 2009 Apr 15;105(8):084112.
17. Takenaka T., Maruyama K., Sakata K. ($Bi_{1/2}$ $Na_{1/2}$)TiO_3-$BaTiO_3$ System for Lead-Free Piezoelectric Ceramics. Jpn J Appl Phys. IOP Publishing; 1991 Sep 30;30(Part 1, No. 9B):2236–9.

18. Fu P., Xu Z., Chu R., Li W., Zang G., Hao J. Piezoelectric, ferroelectric and dielectric properties of La2O3-doped ($Bi_{0.5}Na_{0.5}$)0.94Ba0.06TiO_3 lead-free ceramics. Mater Des. 2010;31(2):796–801.

19. Cerderias E. Materiales piezoeléctricos derivados del (Bi0.5Na0.5)TiO3-BaTiO3 : Preparación y estudio de las propiedades funcionales. 2016;

20. Nakamoto K. Infrared and Raman Spectra of Inorganic and Coordination Compounds. 6th editio. John Wiley & Sons, editor. 2009.

21. Jones G.O., Thomas P.A. Investigation of the structure and phase transitions in the novel A-site substituted distorted perovskite compound Na0.5Bi0.5TiO3. Acta Crystallogr Sect B Struct Sci. International Union of Crystallography; 2002;58(2):168–78.

22. Picht G., Töpfer J., Hennig E. Structural properties of ($Bi_{0.5}Na_{0.5}$)1-xBaxTiO_3 lead-free piezoelectric ceramics. J Eur Ceram Soc. Elsevier Ltd; 2010;30(16):3445–53.

23. Chen C.S., Tu C.S., Chen P.Y., Ting Y., Chiu S.J., Hung C.M., et al. Dielectric properties in lead-free piezoelectric ($Bi_{0.5}Na_{0.5}$)TiO_3–$BaTiO_3$ single crystals and ceramics. J Cryst Growth. 2014;393(0):129–33.

24. R. D. Shannon. Revised Effective Ionic Radii and Systematic Studies of Interatomic Distances in Halides and Chalcogenides. Acta Crystallogr Sect A. :751–67.

25. Fullman J.W.C. and R.L. On the Use of Lineal Analysis for Obtaining Particle Size Distribution Functions in Opaque Samples. J Met. 1956;8:610.

26. Xu C., Lin D., Kwok K.W. Structure, electrical properties and depolarization temperature of ($Bi_{0.5}Na_{0.5}$)TiO_3-$BaTiO_3$ lead-free piezoelectric ceramics. Solid State Sci. 2008;10(7):934–40.